Journal of Solid State Chemistry 183 (2010) 2343–2351

Contents lists available at ScienceDirect

Journal of Solid State Chemistry

journal homepage: www.elsevier.com/locate/jssc

New ternary rare-earth metal boride carbides $R_{15}B_4C_{14}$ (R=Y, Gd–Lu) containing BC_2 units: Crystal and electronic structures, magnetic properties

Volodymyr Babizhetskyy [a,*], Arndt Simon [a], Hansjürgen Mattausch [a], Kurt Hiebl [b], Chong Zheng [c]

[a] Max-Planck-Institut für Festkörperforschung, Heisenbergstrasse 1, Postfach 800665, D-70569 Stuttgart, Germany
[b] Arbeitsgruppe Neue Materialien, Universität Wien, Währingerstrasse 42, A-1090 Wien, Austria
[c] Department of Chemistry and Biochemistry, Northern Illinois University, DeKalb, IL 60115, USA

ARTICLE INFO

Article history:
Received 7 June 2010
Received in revised form
19 July 2010
Accepted 31 July 2010
Available online 5 August 2010

Keywords:
Rare-earth metal boride carbide
Crystal structure
Electronic structure
Extended Hückel calculations
Rare-earth metal magnetism

ABSTRACT

The ternary rare-earth boride carbides $R_{15}B_4C_{14}$ (R=Y, Gd–Lu) were prepared from the elements by arc-melting followed by annealing in silica tubes at 1270 K for 1 month. The crystal structures of $Tb_{15}B_4C_{14}$ and $Er_{15}B_4C_{14}$ were determined from single crystal X-ray diffraction data. They crystallize in a new structure type in space group $P4/mnc$ ($Tb_{15}B_4C_{14}$: a=8.1251(5) Å, c=15.861(1) Å, Z=2, R_1=0.041 (wR_2=0.088) for 1023 reflections with $I_o > 2\sigma(I_o)$; $Er_{15}B_4C_{14}$: a=7.932(1) Å, c=15.685(2) Å, Z=2, R_1=0.037 (wR_2=0.094) for 1022 reflections with $I_o > 2\sigma(I_o)$). The crystal structure contains discrete carbon atoms and bent CBC units in octahedra and distorted bicapped square antiprisms, respectively. In both structures the same type of disorder exists. One R atom position needs to be refined as split atom position with a ratio 9:1 indicative of a 10% substitution of the neighboring C^{4-} by C_2^{4-}. The actual composition has then to be described as $R_{15}B_4C_{14.2}$. The isoelectronic substitution does not change the electron partition of $R_{15}B_4C_{14}$ which can be written as $(R^{3+})_{15}(C^{4-})_6(CBC^{5-})_4 \bullet e^-$. The electronic structure was studied with the extended Hückel method. The investigated compounds $Tb_{15}B_4C_{14}$, $Dy_{15}B_4C_{14}$ and $Er_{15}B_4C_{14}$ are hard ferromagnets with Curie temperatures T_C=145, 120 and 50 K, respectively. The coercive field B_C=3.15 T for $Dy_{15}B_4C_{14}$ is quite remarkable.

1. Introduction

Binary carbides of rare-earth metals (R) exhibit great structural diversity, containing isolated C atoms, C_2 pairs and C_3 groups coordinated by R atoms. At the metal rich side defect NaCl-type carbides are known with compositions around R_3C, R_2C and R_4C_5. Single carbon atoms are located in octahedral lanthanoid voids in R_3C, in R_2C, and R_4C_5 structures, single carbon atoms coexist with C_2 pairs [1,2]. Several compounds with higher carbon contents have been previously reported with the approximate composition $R_{15}C_{19}$ [3–8], and they were later established for R=Sc, Ho–Lu as the Sc_3C_4-type structure [9] with three different kinds of carbon species: isolated carbon atoms, C_2 and C_3 units, respectively. At the carbon-rich sides of these systems, the compounds R_4C_7, R_2C_3, and RC_2 have been found. The structures of R_2C_3 and RC_2 contain only C_2 units [1], for composition R_4C_7 (R=Y, Ho, Er, Tm, Lu) [10,11] an isolated carbon atom besides C_3 units exists. The structural motif of C_3 units has been observed in a few other examples, such as Mg_2C_3, $Ca_3C_3Cl_2$, and $Sc_5Re_2C_7$ [12–14].

In binary R_xB_y borides, the boron atoms form 2-D or 3-D frameworks [15]. Several ternary rare-earth metal boride carbides $R_xB_yC_z$ have been characterized in recent years. The structures of these phases display a variety of different arrangements of the boron, carbon substructures ranging from 0D-dimentional, 1D-, 2D-B, C networks, as well as interconnected boron icosahedra [16]. 0D-units can have different lengths ranging from 3 to 13 non-metal atoms, in addition, isolated C atoms may coexist. The structural motif of CBC units has been observed in a few structures: $R_5B_4C_5$, Al_3BC_3, Sc_2BC_2, Lu_3BC_3, and $R_5B_2C_5$ [17–22].

In the ternary $R_xB_yC_z$ compounds the CBC units with the C atom in the pyramidal metal atom environment are located in bi-capped square antiprisms. The CBC units are linear or bent. The earlier reported compounds $Y_3C_{4-x}B_x$, $Gd_3C_{4-x}B_x$, and $Ho_3C_{4-x}B_x$ are closely related to the Sc_3C_4-type structure, although crystal structure investigations of these were not performed [9,23,24]. The yttrium and gadolinium containing compounds are stabilized only by addition of small amounts of boron to binary R_3C_4 compositions (R=Y, Gd) [5,23,24], whereas a pure binary Ho_3C_4 as well as R_3C_4 for R=Sc, Er–Lu are known [9]. A ternary compound $Er_{15}B_4C_{16}$ which belongs to the Sc_3C_4-type was found by [40] with chains of octahedra along [001] alternately filled with C and C_2. The CBC unit lies inside a distorted bicapped square antiprism.

* Corresponding author. Fax: +49 711 6891091.
E-mail address: v.babizhetskyy@fkf.mpg.de (V. Babizhetskyy).

0022-4596/$ - see front matter © 2010 Elsevier Inc. All rights reserved.
doi:10.1016/j.jssc.2010.07.046

Here we report on investigations of new members of this structure family.

2. Experimental

2.1. Synthesis and analysis

The samples of $R_{15}B_4C_{14}$ (R=Y, Gd–Lu) were prepared from commercially available pure elements: rare-earth metals with a claimed purity of 99.99 at%, Alfa-Aesar, Johnson Matthey Company, sublimed bulk pieces; crystalline boron powder, purity 99.99 at%, H.C. Starck, Germany; graphite powder, purity 99.98 at%, Aldrich. Before use, the graphite and boron powders were outgased overnight at 1220 K, $p<10^{-5}$ mbar. The rare-earth metals were filed to coarse powders with beryllium bronze files (Dönges GmbH, Germany). Stoichiometric mixtures of the constituents were compacted in stainless steel dies. The pellets were arc-melted under purified argon atmosphere [25] on a water-cooled copper hearth. The alloy buttons of 1 g were turned over and remelted three times to improve homogeneity. The samples were then wrapped in molybdenum foil and annealed in silica tubes under argon for 1 month at 1270 K. The ytterbium containing compound was obtained by high-frequency melting (30 min at 1970 K) of a pellet with somewhat higher ytterbium content in a sealed tantalum tube under argon. The compounds are not stable in air, and sample handling was carried out under argon atmosphere in a glove box or through the Schlenk technique.

Chemical analysis of $Dy_{15}B_4C_{14}$ was performed in the Mikroanalytisches Labor Pascher in Remagen-Bandorf, Germany, and showed: Dy 44.9 at%, B 11.0 at% and C 44.1 at%.

2.2. X-ray diffraction and structure refinement

Small irregularly shaped single crystals were selected from the crushed samples and sealed under argon atmosphere in glass capillaries. These crystals were first examined by the Buerger precession technique in order to establish their suitability for the subsequent data collection. As it turned out most crystals of the title compounds with different R were twinned. Suitable small single crystals of rather irregular shape were found in the terbium and erbium containing samples. The single crystals diffraction data of $Tb_{15}B_4C_{14}$ and $Er_{15}B_4C_{14}$ were collected at room temperature on a STOE IPDS I image plate diffractometer with monochromatized Ag$K\alpha$ radiation. A numerical absorption correction for $Tb_{15}B_4C_{14}$ was made on the basis of the crystal shape [26]. All relevant crystallographic data are listed in Table 1. The starting atomic parameters were derived via direct methods using the program SIR97 [27]. These were subsequently refined with the program SHELX-97 [28] within the WinGX program package [29] (full matrix least-squares on F^2) with anisotropic atomic displacements for R atoms. The atomic coordinates and isotropic displacement parameters are listed in Table 2. The refinements converged well, but they indicated some inconsistencies for Tb2 atoms. The light atoms could be located from the difference Fourier maps. The anisotropic displacement parameters of the Tb2 atoms show large values along the c direction. We therefore refined these atoms with split position Tb2/Tb5 and occupation factors for Tb2 sof=0.906(6) and for Tb5 sof=0.094(6). Final anisotropic displacement parameters for the terbium atoms in $Tb_{15}B_4C_{14}$ are listed in Table 4, and selected interatomic distances are reported in Table 6. In order to verify the disorder in $Tb_{15}B_4C_{14}$ a suitable single crystals of $Er_{15}B_4C_{14}$ was measured. The result of the refinement hardly differs from that of the Tb compound. Data are summarized in Tables 1, 3 and 5.

Table 1
Crystal data and structure refinement for $Tb_{15}B_4C_{14}$ and $Er_{15}B_4C_{14}$.

Empirical formula	$Tb_{15}B_4C_{14}$	$Er_{15}B_4C_{14}$
Crystal system	Tetragonal	Tetragonal
Space group	$P4/mnc$ (no. 128)	$P4/mnc$ (no. 128)
Pearson symbol, Z	tP66, 2	tP66, 2
Lattice parameters		
a (Å)	8.1251(5)	7.932(1)
c (Å)	15.861(1)	15.685(2)
Unit cell volume (Å^3)	1047.1(1)	986.8(2)
Calculated density (g/cm^3)	8.231	9.155
Absorption coefficient (1/cm)	26.58	33.76
Crystal size (mm^3)	$0.20\times0.04\times0.10$	$0.22\times0.04\times0.18$
Radiation and wavelength (Å)	Ag$K\alpha$, 0.56086	Ag$K\alpha$, 0.56086
Diffractometer	STOE IPDS I	STOE IPDS I
Refined parameters	34	34
Refinement	F^2	F^2
$2\theta_{max}$ and $(\sin\theta/\lambda)_{max}$	56.16, 0.837	60.96, 0.904
h, k, l	$-13<h<13$	$-14<h<14$
	$-13<k<13$	$-13<k<13$
	$-26<l<26$	$-28<l<28$
Collected reflections	17,983	19,136
Independent reflections	1340 (R_{int}=0.089)	1502 (R_{int}=0.145)
Reflections with $I_o\geq2\sigma(I_o)$	1023 (R_σ=0.029)	1022 (R_σ=0.045)
Final R_1 indices (R_1 all data)	0.041 (0.057)[a]	0.037 (0.063)[a]
Weighted wR_2 factor(wR_2 all data)	0.088 (0.093)[b]	0.085 (0.094)[c]
Goodness-of-fit on F^2	1.21	1.04
Largest diff. peak and hole (e Å^{-3})	4.0/−3.5[d]	5.0/−3.6[d]

[a] $R_1(F)=[\Sigma(|F_o|-|F_c|)]/\Sigma|F_o|$.
[b] $wR_2(F^2)=[\Sigma[w(F_o^2-F_c^2)^2/\Sigma[w(F_o^2)^2]]^{1/2}$, $w^{-1}=\sigma^2(F_o)^2+(0.034)^2+35.64P]$, where $P=(F_o^2+2F_c^2)/3$.
[c] $wR_2(F^2)=[\Sigma[w(F_o^2-F_c^2)^2/\Sigma[w(F_o^2)^2]]^{1/2}$, $w^{-1}=\sigma^2(F_o)^2+(0.048)^2+0.00P]$, where $P=(F_o^2+2F_c^2)/3$.
[d] Position close ~0.9 Å to that of the $R3$/$R4$ atoms.

Table 2
Atomic coordinates and displacement parameters (in Å^2) for $Tb_{15}B_4C_{14}$.

Atom	Site	Occ.	x	y	z	U_{eq}/U_{iso}
Tb1	2a	1.00	0	0	0	0.0019(1)
Tb2	4e	0.906(6)	0	0	0.3138(1)	0.0026(3)
Tb3	8h	1.00	0.39895(6)	0.19203(6)	0	0.0017(1)
Tb4	16i	1.00	0.10162(5)	0.29591(5)	0.14938(2)	0.0021(1)
Tb5	4e	0.094(6)	0	0	0.3434(1)	0.0026(3)
C1	4e	1.00	0	0	0.162(1)	0.010(3)
C2	8h	1.00	0.696(1)	0.103(1)	0	0.005(2)
C3	16i	1.00	0.401(1)	0.199(1)	0.1671(5)	0.006(1)
B	8g	1.00	0.345(1)	0.155(1)	1/4	0.004(1)

Table 3
Atomic coordinates and displacement parameters (in Å^2) for $Er_{15}B_4C_{14}$.

Atom	Site	Occ.	x	y	z	U_{eq}/U_{iso}
Er1	2a	1.00	0	0	0	0.0009(1)
Er2	4e	0.92(1)	0	0	0.3132(2)	0.0019(3)
Er3	8h	1.00	0.40122(5)	0.19473(5)	0	0.0024(1)
Er4	16i	1.00	0.10124(3)	0.29213(3)	0.14810(2)	0.0010(1)
Er5	4e	0.08(1)	0	0	0.3336(2)	0.0019(3)
C1	4e	1.00	0	0	0.1595(8)	0.002(1)
C2	8h	1.00	0.696(1)	0.107(1)	0	0.005(2)
C3	16i	1.00	0.4029(9)	0.1990(7)	0.1668(5)	0.003(2)
B	8g	1.00	0.3474(9)	0.1526(9)	1/4	0.003(1)

X-ray powder diffraction patterns for the full profile refinement of $Dy_{15}B_4C_{14}$ were collected on a powder diffractometer STOE STADI P with monochromated Mo$K\alpha_1$ radiation ($5^\circ\leq2\theta\leq75^\circ$, step size 0.1°, measurement time per step: 200 s). For the profile refinement the programs WinPLOTR and Fullprof have been used

Table 4
Anisotropic displacement parameters for terbium atoms in $Tb_{15}B_4C_{14}$.

Atom	U_{11}	U_{22}	U_{33}	U_{23}	U_{13}	U_{12}
Tb1	0.0020(3)	0.0020(3)	0.0063(4)	0.000	0.000	0.000
Tb2	0.0026(2)	0.0026(2)	0.0115(9)	0.000	0.000	0.000
Tb3	0.0024(2)	0.0041(2)	0.0071(3)	0.000	0.000	0.0009(1)
Tb4	0.0024(2)	0.0061(2)	0.0075(2)	−0.0003(1)	0.00004(13)	0.0011(1)
Tb5	0.0026(2)	0.0026(2)	0.0115(9)	0.000	0.000	0.000

Table 5
Anisotropic displacement parameters for erbium atoms in $Er_{15}B_4C_{14}$.

Atom	U_{11}	U_{22}	U_{33}	U_{23}	U_{13}	U_{12}
Er1	0.0004(2)	0.0004(2)	0.0006(3)	0.000	0.000	0.000
Er2	0.0015(1)	0.0015(1)	0.0026(8)	0.000	0.000	0.000
Er3	0.0005(2)	0.0053(2)	0.0013(2)	0.000	0.000	0.0006(1)
Er4	0.0002(1)	0.0014(1)	0.0013(1)	−0.0004(1)	−0.0001(1)	0.0004(1)
Er5	0.0015(1)	0.0015(1)	0.0026(8)	0.000	0.000	0.000

Table 6
Interatomic distances (Å) in the structure of $Tb_{15}B_4C_{14}$.

Atoms	Distance	Atoms	Distance	Atom	Distance
Tb1–2C1	2.57(2)	Tb3–2Tb5	3.620(1)	C1–Tb2	2.41(2)
Tb1–4C2	2.61(1)	Tb3–2Tb3	3.7247(8)	C1–4Tb4	2.550(2)
Tb1–8Tb3	3.4750(4)			C1–Tb5	2.88(2)
Tb1–4Tb3	3.5972(6)	Tb4–C2	2.3701(5)		
		Tb4–C1	2.550(2)	C2–2Tb4	2.3701(5)
Tb2–C1	2.41(2)	Tb4–C3	2.570(9)	C2–2Tb3	2.52(1)
Tb2–4C3	2.585(8)	Tb4–C3	2.604(9)	C2–Tb3	2.57(1)
Tb2–B7	2.80(1)	Tb4–C3	2.609(8)	C2–Tb1	2.608(8)
Tb2–4Tb4	3.643(1)	Tb4–B	2.656(6)		
Tb2–4Tb4	3.6833(5)	Tb4–Tb4	3.4024(5)	C3–B1	1.438(8)
Tb2–4Tb3	3.956(1)	Tb4–Tb3	3.4649(6)	C3–1Tb4	2.57(1)
		Tb4–Tb3	3.4872(6)	C3–Tb5	2.572(9)
Tb3–2C2	2.52(1)	Tb4–Tb3	3.5071(6)	C3–Tb2	2.585(8)
Tb3–C2	2.57(1)	Tb4–2Tb4	3.5951(6)	C3–2Tb4	2.61(1)
Tb3–2C3	2.651(8)	Tb4–Tb2	3.643(1)	C3–Tb3	2.650(8)
Tb3–2Tb4	3.4649(6)	Tb4–Tb4	3.7050(6)		
Tb3–2Tb4	3.4872(6)			B–2C3	1.438(8)
Tb3–2Tb4	3.5072(6)	Tb5–4C3	2.572(9)	B–2Tb4	2.655(5)
Tb3–Tb3	3.5261(8)	Tb5–C1	2.88(2)	B–2Tb4	2.79(1)
Tb3–Tb1	3.5072(6)				

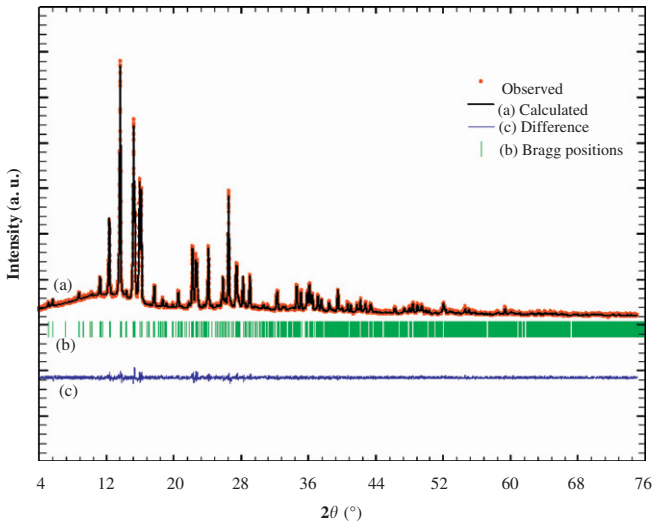

Fig. 1. Comparison of observed and calculated X-ray powder profiles for $Dy_{15}B_4C_{14}$.

[30,31]. For the X-ray powder structure refinement of the $Dy_{15}B_4C_{14}$ the structural model of $Tb_{15}B_4C_{14}$ compound was used. Fig. 1 shows the final fit of the calculated pattern to the observed one. Details of the refinement are summarized in Table 7 and final atom parameters are given in Table 8.

The calculated X-ray powder diffraction patterns were found to be in good agreement with the experimental patterns of all phases $R_{15}B_4C_{14}$ (R=Y, Gd–Lu) recorded as described for the Dy compound. The composition $R_{15}B_4C_{14}$ for the isostructural series was used, although in earlier investigations the cell parameters from powders for some of these compounds were assigned to $Y_3C_{4-x}B_x$, $Gd_3B_{4-x}C_x$ and $Ho_3B_{4-x}C_x$ [5,23,24]. The unit cell parameters from powder data, refined with the CSD program package [32], are given in Table 9. The correct indexing of the X-ray powder patterns was ensured through intensity calculations using the atomic positions from the single crystal refinement.

Table 7
Crystal data of the X-ray powder structure refinement for the $Dy_{15}B_4C_{14}$.

Space group	*P4/mnc* (no. 128)
Lattice parameters	
a (Å)	8.0882(1)
c (Å)	15.8846(3)
Cell volume (Å^3)	1039.16(5)
Number of atoms in cell	66
Calculated density (g/cm^3)	8.465(1)
Diffractometer	STOE STADI P
Radiation	Mo$K\alpha_1$
Mode of refinement	Full matrix full profile data refinement
Number of atom sites	8
Number of free parameters	23
2ϑ limits	4–75
R_{Bragg}, R_p, R_{wp}	0.021, 0.115, 0.103,
R_{exp}, χ	0.091, 1.27

Table 8
Atomic coordinates and displacement parameters (in Å^2) for $Dy_{15}B_4C_{14}$.

Atom	Site	Occ.	*x*	*y*	*z*	U_{eq}/U_{iso}
Dy1	2*a*	1.00	0	0	0	0.008(1)
Dy2	4*e*	0.91(1)	0	0	0.3113(2)	0.010(1)
Dy3	8*h*	1.00	0.4002(3)	0.1934(3)	0	0.015(1)
Dy4	16*i*	1.00	0.1018(3)	0.2956(2)	0.14934(8)	0.012(1)
Dy5	4*e*	0.09(1)	0	0	0.3369(2)	0.010(1)
C1	4*e*	1.00	0	0	0.157(1)	0.014(6)
C2	8*h*	1.00	0.680(5)	0.106(5)	0	0.009(4)
C3	16*i*	1.00	0.384(4)	0.213(4)	0.169(1)	0.011(2)
B	8*g*	1.00	0.358(7)	0.142(7)	1/4	0.011(2)

Table 9
Unit cell parameters (powder data) for $R_{15}B_4C_{14}$ (R=Y, Tb–Lu).

Compound	*a* (Å)	*c* (Å)	*V* (Å^3)
$Y_{15}C_4B_{14}$	8.0503(6)	16.041(1)	1039.6(2)
$Gd_{15}B_4C_{14}$	8.2103(6)	16.096(1)	1085.0(3)
$Tb_{15}B_4C_{14}$	8.1451(2)	15.913(1)	1055.7(1)
$Dy_{15}B_4C_{14}$	8.0882(1)	15.884(1)	1039.2(1)
$Ho_{15}B_4C_{14}$	7.9980(6)	15.854(1)	1020.6(3)
$Er_{15}B_4C_{14}$	7.9575(8)	15.686(2)	993.2(3)
$Tm_{15}B_4C_{14}$	7.9214(8)	15.751(2)	988.3(5)
$Yb_{15}B_4C_{14}$	7.819(1)	15.728(2)	961.5(5)
$Lu_{15}B_4C_{14}$	7.8225(8)	15.603(2)	954.8(2)

2.3. Theoretical calculations

The density of states (DOS) and the crystal orbital overlap population (COOP) [33] curves were computed using the tight-binding extended Hückel method (EH) [34,35] with 40k-points in the irreducible wedge of the Brillouin zone. The EH parameters used are (orbital energy in eV and exponent in parentheses): Tb 6*s*: −6.09(1.42), 6*p*: −4.81(1.42), 5*d*: −6.09(2.77 and 1.25, with expansion coefficients 0.7135 and 0.4590); C 2*s*: −21.4(1.625), 2*p*: −11.4 (1.625); B 2*s*: −15.2(1.3), 2*p*: −8.5(1.3).

2.4. Magnetic properties

Magnetizations M and the magnetic susceptibilities, $\chi = M/H$, in external fields $B \leq 7$ T were studied in the temperature interval 1.8–300 K using a MPMS XL-7 SQUID magnetometer (Quantum Design, Inc.).

3. Results and discussion

3.1. Structure chemistry

The crystal structure of the new ternary compound $R_{15}B_4C_{14}$ (Fig. 2) is closely related to that of the Sc_3C_4-type described by Pöttgen and Jeitschko [9]. It is interesting to observe the formation of isostructural phases $R_{15}B_4C_{14}$ (R=Y, Gd–Lu) previously described as $R_3B_xC_{4-x}$ (observed for R=Y, Gd and Ho) [5,23,24], whereas the pure binary carbides R_3C_4 were not found for R=Y, Gd, Tb, and Dy.

The structure of $Tb_{15}B_4C_{14}$ is composed of two kinds of slabs formed from bilayers of metal atoms with nonmetal atoms in between. One kind contains bent CBC units and discrete C atoms (C1) whereas the other contains only octahedrally coordinated C atoms (C2). The main difference between the $Tb_{15}B_4C_{14}$ and Sc_3C_4-type structure lies in the fact that there are empty octahedral voids in the former which are occupied by C_2 units in the latter.

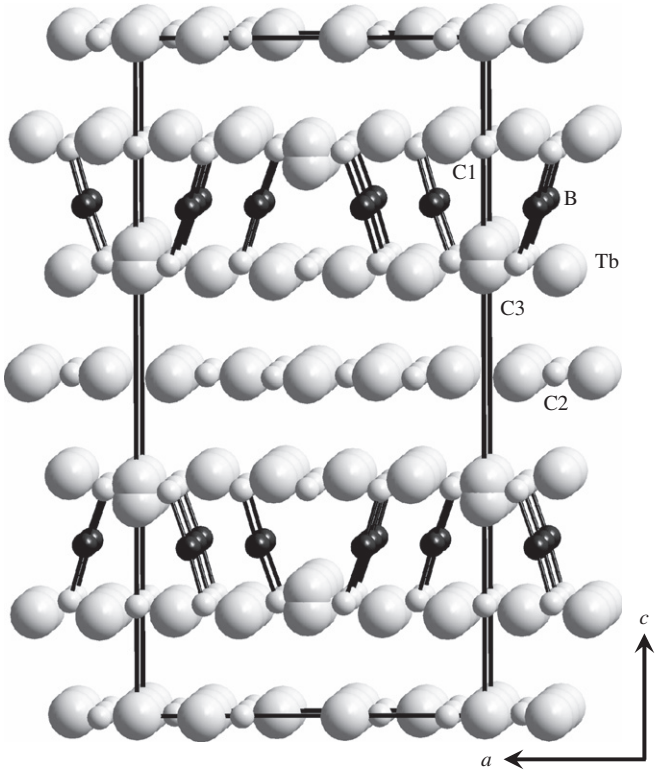

Fig. 2. Crystal structure of $Tb_{15}B_4C_{14}$.

The CBC unit lies inside a distorted bicapped square antiprism formed by 10 Tb atoms. The C–B–C bond angle is 174.9(5)°, and the two C3–B distances are 1.438(8) Å. These triatomic CBC units in $Tb_{15}B_4C_{14}$ have the same environment as the C_3 units in the Sc_3C_4 structure with the central C atoms being substituted by boron atoms in $Tb_{15}B_4C_{14}$. For comparison, the C–C distances in the C_3 unit are 1.34 Å and C–C–C bond angle is 175.8°.

The single octahedrally surrounded carbon atoms C1 and C2 in $Tb_{15}B_4C_{14}$ exhibit Tb–C distances ranging from 2.370(1) Å (C2–Tb4) to 2.608(8) Å (C2–Tb1).

The slab containing single carbon atoms and CBC units also forms the characteristic structural feature of ternary rare-earth boride carbides belonging to the $Gd_5B_2C_5$ type [22] where the B–C distances are 1.46 Å and $Tb_{10}B_7C_{10}$ type [36] with B–C distances ranging from 1.46 to 1.50 Å. Bent CBC units are present in quarternary phases, such as $La_9Br_5B_3C_6$ [37], $La_4I_5B_2C$ [38], and $La_3Br_2BC_2$ [38].

Discrete linear CBC units have been observed in the structure type of $Gd_4B_3C_4$ [36,39], and they are also known for other ternary rare-earth metal boride carbides Sc_2BC_2 [19,20], and Lu_3BC_3 [21], where the B–C distances are 1.48, 1.48, and 1.44 Å, respectively. In the ternary compound Lu_3BC_3, the slabs centered by CBC units are separated by slabs containing single carbon atoms, and in the structure of $Gd_4B_3C_4$ the slabs containing linear CBC units are separated by slabs centered by infinite $(BC)_\infty$ branched chains.

Our attempt to refine the structure of $Tb_{15}B_4C_{14}$ with C_2 units in the octahedral voids formed from $4 \times$ Tb3 (equatorial) and $2 \times$ Tb2 (apical) as in the Sc_3C_4 structure was not successful. There is no scattering density inside this void, neither in the center according to a single C atom, nor off-center as expected for a C_2 dumbbell. As a strange feature the apical Tb2 position exhibits a disorder which needs a description with a split position. The refinement leads to a site occupation of 90% for Tb2 and 10% for the split atom Tb5.

To be sure that this disorder is no artefact due to poor diffraction data, a single crystal investigation of the isotypic Er compound was performed. The result of the refinement hardly differs from that of the Tb compound. In both structures the octahedron formed from Tb4 (equatorial) and Tb1, Tb2 (Tb5) (apical) is occupied by an atom that refines as C1. However, the split position Tb2/Tb5 with 10% of an elongated octahedron gives indirect evidence for a 10% substitution of C1 by a C_2 unit. Such an extent of substitution is beyond the limit of detection. The elongation of the octahedron only shows up with Tb5 as Tb1 is symmetrically coordinated by C/C_2 entities.

For an idealized composition $Tb_{15}B_4C_{14}$ the electron partitioning can be described as $(Tb^{3+})_{15}(C^{4-})_6(CBC^{5-})_4 \bullet e^-$. The disorder actually changes the composition slightly according to $(Tb^{3+})_{15}(C^{4-})_4(C^{4-})_{0.9}(C_2^{4-})_{0.1})_2\,(CBC^{5-})_4 \bullet e^- \cong Tb_{15}B_4C_{14.2}$. This marginal deviation from the idealized composition has no significant influence on the electronic structure calculations and magnetic measurements described in the following.

Details of compositional and structural relationships between Sc_3C_4 and $R_{15}B_4C_{14+x}$ need further investigations. In a slightly different preparation approach – no premelting – Oeckler isolated a phase $Er_{15}B_4C_{16}$ which belongs to the Sc_3C_4-type structure with chains of octahedra along [001] alternately filled with C and C_2 in contrast to the phase described here with empty octahedra alternating with those filled 90% C and 10% C_2 [41]. The difference in composition shows up in an elongation of the *c*-axis in the case of $Er_{15}B_4C_{16}$ as expected. It remains to be analyzed whether both phases belong to the same range of homogeneity.

3.2. Electronic structure

The molecular orbital overlap population (MOOP) [40] plot calculated via the extended Hückel method for the C–B bond of the CBC unit in $Tb_{15}B_4C_{14}$ is shown in Fig. 3. The point group symmetry of the CBC unit is C_{2v}, and the orbitals are labeled accordingly. The degeneracy of the π levels for a linear unit is removed. Nevertheless, the main feature of a linear unit remains. There are 8 bonding orbitals which can accommodate 16 electrons, resulting in a charge state of CBC^{5-} which is isoelectronic to CO_2. In other words, the charge can be formally distributed according to: $C^{2-}=B^{-}=C^{2-}$. The electron partitioning for both $Tb_{15}B_4C_{14}$ and $Er_{15}B_4C_{14}$ yields a single "free" electron delocalized among the Tb 5*d* orbitals in metal–metal bonding.

Fig. 4 shows the crystal overlap population (COOP) curves for representative bonds calculated for the $Tb_{15}B_4C_{14}$ structure. For the C–B COOP curve, the orbital energy ordering of the isolated CBC unit is still obvious. The peak at -22 eV corresponds to the $1a_1$ orbital of the CBC unit. At -14.5 eV the $1b_1$ level occurs. The large peak above the $1b_1$ level contains the remaining bonding orbitals of the CBC unit. Due to the extended interaction with Tb, these orbitals have significant dispersions so that their peaks overlap with each other to create a large bonding peak below the Fermi level. Below the Fermi level, all states contribute to C–B, Tb–B, Tb–C and Tb–Tb bonding except for two small peaks in the Tb–B COOP. These are actually nonbonding states because the scale in this COOP is much finer than that of the C–B COOP.

The single "free" electron occupies a small portion of the Tb–Tb bonding states. Adding more electrons would strengthen the Tb–Tb bonding. However, it will also populate the C–B antibonding state. Therefore a single "free" electron seems to the optimal electron count for $Tb_{15}B_4C_{14}$. Replacing B by C would destabilize the structure. Our extended Hückel calculation showed that replacing 2, 4, and 8 B by C in the 8 CBC units of the unit cell will cause the average C–B and C–C overlap population to decrease from 1.29 to 1.22, 1.19, 1.12, respectively.

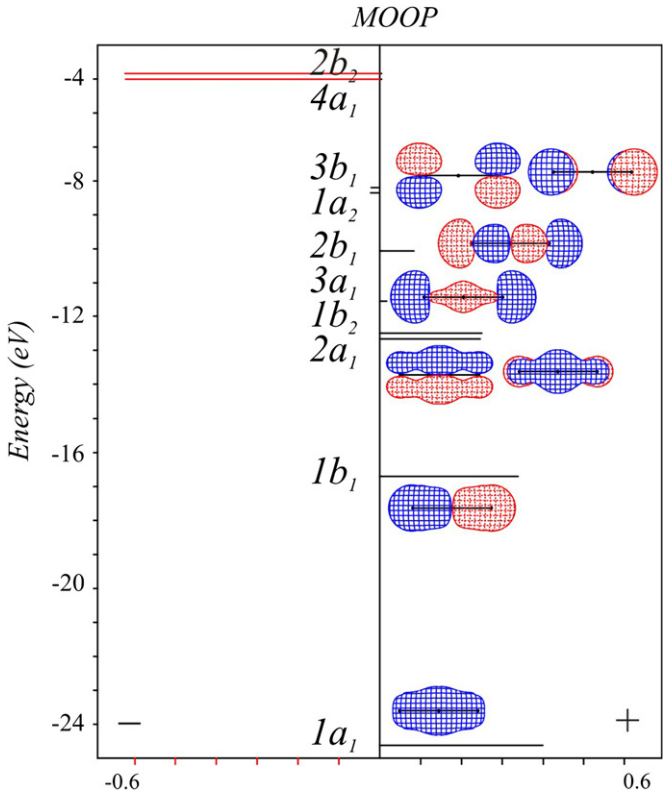

Fig. 3. Extended Hückel calculated molecular orbital overlap population (MOOP) plot for the C–B bond of the CBC unit inside $Tb_{15}C_{14}B_4$.

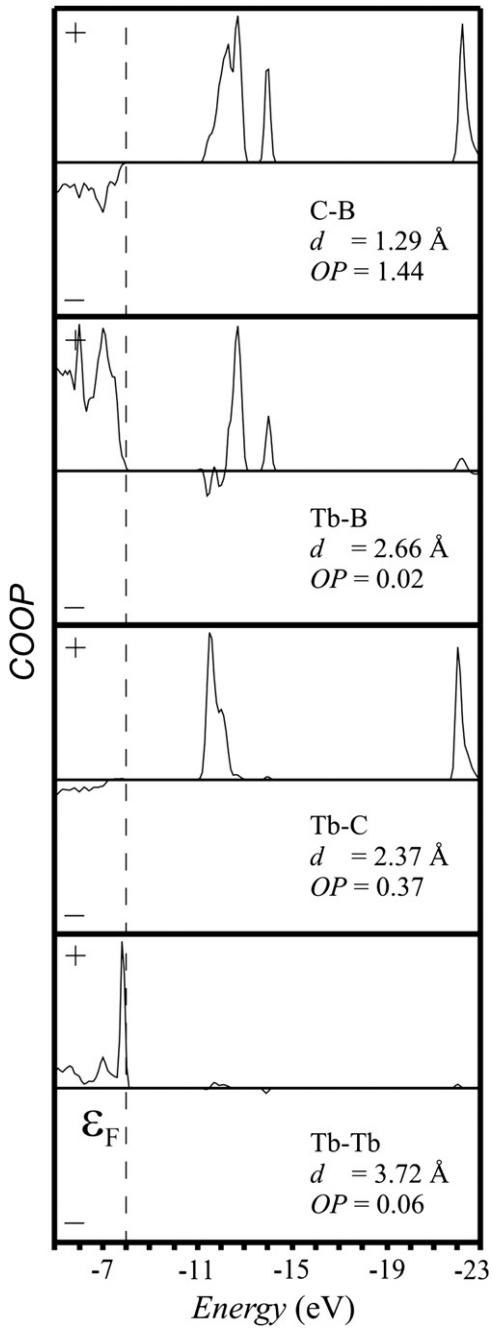

Fig. 4. Calculated EH COOP for $Tb_{15}B_4C_{14}$.

Table 10
Magnetic data of $R_{15}B_4C_{14}$.

Compound	μ_{eff} (μ_B)	θ_p (K)	T_C (K)	μ_S (μ_B)	M_S (A m^2/kg)	M_R (A m^2/kg)	B_C (T)
$Tb_{15}B_4C_{15}$	9.8	140.9	145	6.4	207	172	1.95
$Dy_{15}B_4C_{15}$	10.6	121.4	120	6.5	206	189	3.15
$Er_{15}B_4C_{15}$	9.3	41.8	50	6.4	197	93	0.48

M_S—saturation magnetization, M_R—remnant magnetization, B_C—coercive field.

3.3. Magnetism

The results of the magnetic measurements of the compounds with idealized formulas $R_{15}B_4C_{14}$ (R=Tb, Dy, Er) are summarized in Table 10 and Figs. 5–10. For the paramagnetic regime ($T > 200$ K) we have fitted the susceptibility data measured in an external field, $B=7$ T, according to a simple linear Curie–Weiss law shown as solid and dashed lines in Figs. 5–7. The derived values of the effective moments, μ_{eff}, agree well with the theoretical moments of the R^{3+} ions and are listed together with the asymptotic paramagnetic Curie temperatures, θ_p, in Table 10.

At temperatures lower than 150 K all the three compounds undergo ferromagnetic transitions, for ordering temperatures see Table 10. The temperature dependencies of the magnetization, $M(T)$, as shown in Figs. 8–10, reveal pronounced differences of the zero field cooled (zfc) plot in rising temperatures, and the field cooled (fc) plot. The origin of such a behavior is due to the presence of narrow domain walls. At the lowest temperature the net magnetization of the zfc samples is small due to the fact that the thermal energy is not sufficient to move the narrow walls. $M(T)$ strongly rises with increasing temperatures, passes a maximum and falls off near the Curie temperature, T_C. As the wall movement is hampered at low temperature, a high net magnetization depending on the applied field is frozen in upon subsequent cooling of the sample. The isothermal magnetization plots at $T=2$ K presented in the insets of Figs. 5–7 prove the presence of narrow walls by practically field independence of the first part of the initial magnetization curve. The presence of an energy barrier prevents wall movement up to a critical field which is close to the coercive field [42]. The values of the saturation moments, μ_S, were calculated from the saturation magnetization data, M_S, at a field of $B=7$ T and are listed together with the values of the coercive fields B_C and the remnant magnetization M_R in Table 10. The reduced values for $\mu_S \leq 2/3$ gJ are attributed to the magnetic anisotropy (easy plane or easy axis) in bulk samples. We note that the coercive field of the Dy containing sample is quite remarkable. In an earlier work on the related system $Ho_3C_{4-x}B_x$ [24], the pure binary carbide was found to order antiferromagnetically at $T=10$ K. Addition of boron has two effects: (a) the magnetic order of the ternary compound changes to ferromagnetism and, (b) the ordering temperatures rise to $T_C=30$ K with increasing boron content ($x_{max}=0.8$) as well as the magnetic hardness due to the presence of narrow domain walls. Hence, we have to assume that the boron atoms act as pinning centers for the walls.

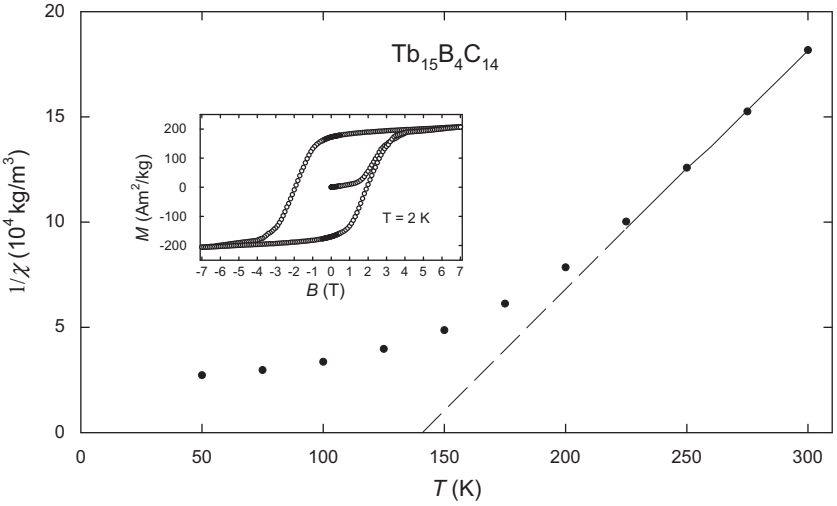

Fig. 5. Reciprocal susceptibility versus temperature for $Tb_{15}B_4C_{14}$. Solid and dashed line C–W fit. Inset: Isothermal magnetization versus applied field at $T=2$ K.

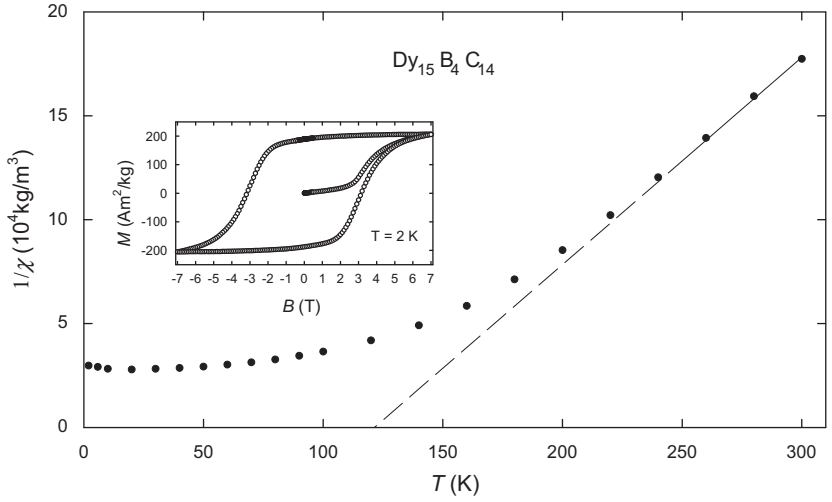

Fig. 6. Reciprocal susceptibility versus temperature for $Dy_{15}B_4C_{14}$. Solid and dashed line C–W fit. Inset: Isothermal magnetization versus applied field at $T=2$ K.

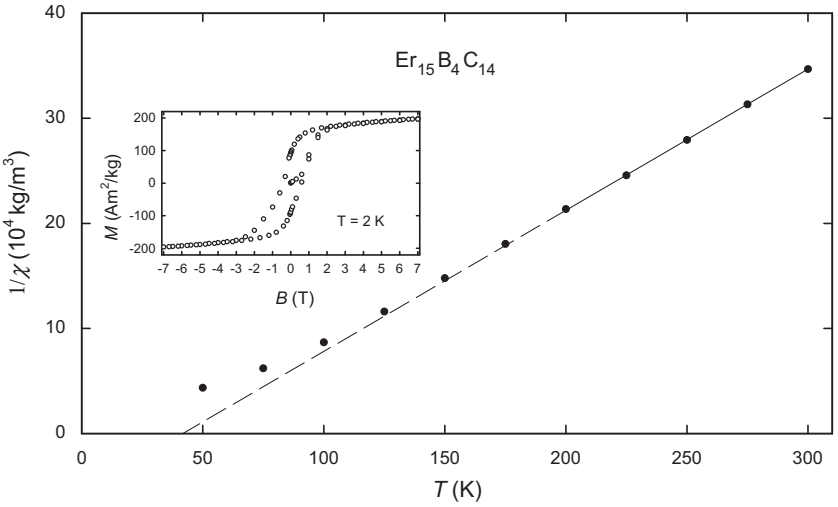

Fig. 7. Reciprocal susceptibility versus temperature for $Er_{15}B_4C_{14}$. Solid and dashed. Line C–W fit. Inset: Isothermal magnetization versus applied field at $T=2$ K.

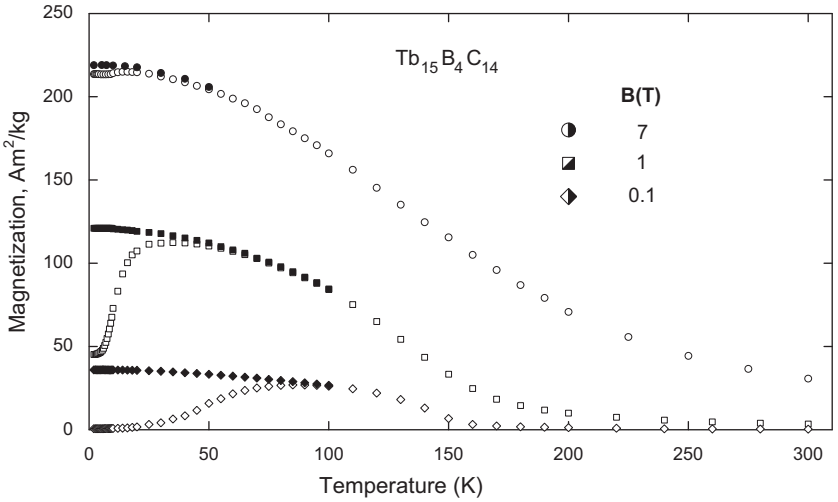

Fig. 8. Magnetization versus temperature for $Tb_{15}B_4C_{14}$ at various external fields. Open symbols in increasing, filled symbols in decreasing temperature.

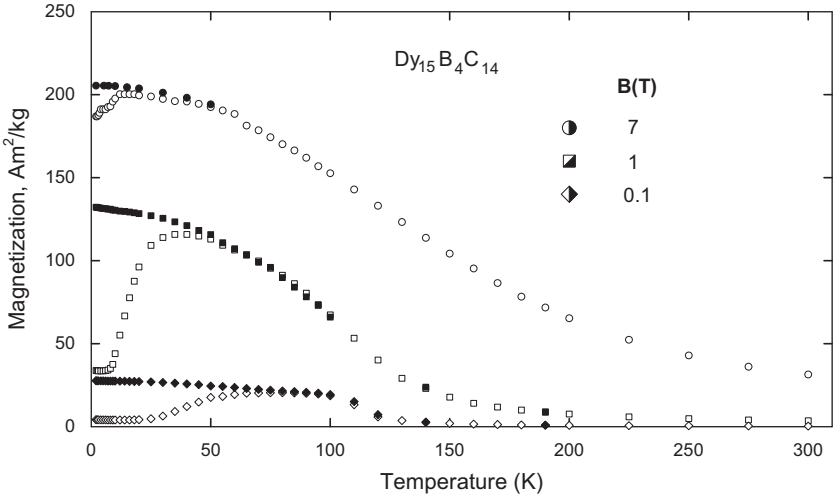

Fig. 9. Magnetization versus temperature for $Dy_{15}B_4C_{14}$ at various external fields. Open symbols in increasing, filled symbols in decreasing temperature.

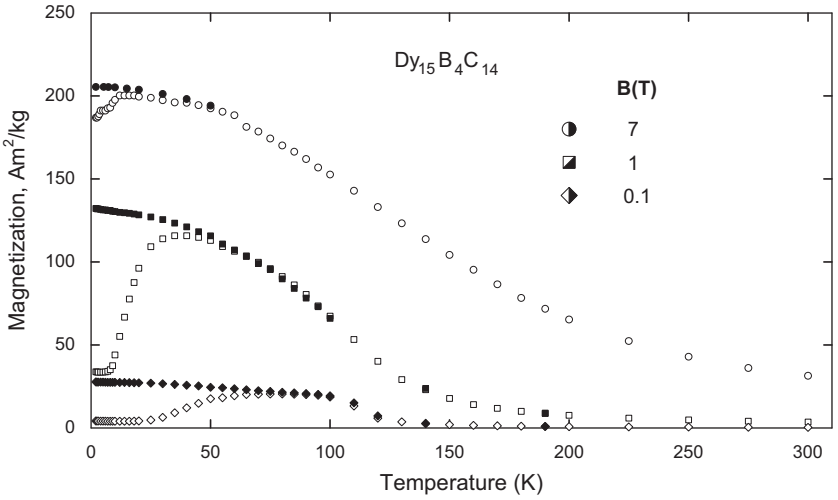

Fig. 10. Magnetization versus temperature for $Er_{15}B_4C_{14}$ at various external fields. Open symbols in increasing, filled symbols in decreasing temperature.

4. Conclusion

The ternary rare earth boride carbides $R_{15}B_4C_{14}$ (R=Y, Gd–Lu) were prepared from the elements by arc-melting followed by annealing in silica tubes at 1270 K for 1 month. $Tb_{15}B_4C_{14}$ is a new member of the rare-earth metal boride carbide series in which the finite quasi-molecular CBC entities as well as isolated C atoms are embedded in the voids of the metal atom matrix. The structure of $Tb_{15}B_4C_{14}$ contains two types of slabs filled with B and C atoms. One slab contains finite bent CBC units and isolated carbon atoms whereas another is formed only from octahedral coordinated single carbon atoms. One single carbon atom position is substituted by 10% of C_2 units which changes the actual composition slightly to $Tb_{15}B_4C_{14.2}$ but leaves the electron balance unchanged in case of C_2^{4-}. The electronic structure for the idealized composition corresponds to an electron partitioning according to $(Tb^{3+})_{15}(C^{4-})_6(CBC^{5-})_4\bullet e^-$ giving rise to a single electron per formula for Tb–Tb framework bonding. The magnetism of the ternary rare earth boride carbides $R_{15}B_4C_{14}$ (R=Tb, Dy, Er) is characterized by the onset of ferromagnetic order below $T<150$ K. The Dy containing compound appears to be an extremely hard-magnetic material.

Supplemental Information

Further details of the crystal structure investigation can be obtained from the Fachinformationszentrum Karlsruhe, 76344 Eggenstein-Leopoldshafen, Germany (fax: (49)7247-808-666; E-mail: crystdata@fiz-karlsruhe.de) on quoting the depository numbers CSD-421868 for $Tb_{15}B_4C_{14}$ and 421867 for $Er_{15}B_4C_{14}$

Acknowledgments

The authors gratefully thank M. Babizhetska for the sample preparation, Dr. C. Hoch for X-ray intensity data collection, and E. Brücher for the magnetization measurements.

References

[1] G.-Y. Adachi, N. Imanaka, Z. Fuzhong, in: K.A. Gschneidner Jr, L. Eyring (Eds.), Handbook on the Physics and Chemistry of Rare Earths, Elsevier Science Publishers1991, pp. 61–189.
[2] R. Czekalla, T. Hüfken, W. Jeitschko, R.-D. Hoffmann, R. Pöttgen, J. Solid State Chem. 132 (1997) 294–299.
[3] H. Jedlicka, H. Nowotny, F. Benesovsky, Monatsh. Chem. 102 (1971) 389–403.
[4] B. Hájek, P. Karen, V. Brožek, J. Less-Common Met. 96 (1984) 35–48.
[5] J. Bauer, H. Nowotny, Monatsh. Chem. 102 (1971) 1129–1145.
[6] J. Bauer, J. Less-Common Met. 37 (1974) 161–165.
[7] J. Bauer, H. Bienvenu, C.R. Seances, Acad. Sci. Ser. 290 (1980) 387–390C 290 (1980) 387–390.
[8] J. Bauer, J.D. Ansel, J. Less-Common Met. 109 (1985) L9.
[9] R. Pöttgen, W. Jeitschko, Inorg. Chem. 30 (1991) 427–431.
[10] R. Czekalla, W. Jeitschko, R.-D. Hoffmann, H. Rabeneck, Z. Naturforsch. 51b (1996) 646–654.
[11] Hj. Mattausch, T. Gulden, R.K. Kremer, J. Horakh, A. Simon, Z. Naturforsch. 49b (1994) 1439–1443.
[12] H. Fjellvåg, P. Karen, Inorg. Chem. 31 (1992) 3260–3263.
[13] H.-J. Meyer, Z. Anorg. Allg. Chem. 593 (1991) 185–192.
[14] R. Pöttgen, W. Jeitschko, Z. Naturforsch. 47b (1992) 358–364.
[15] Yu Kuz'ma, in: Crystal Chemistry of Borides, Vyshcha Shkola, Lwiw, 1983 p. 164.
[16] J. Bauer, J.-F. Halet, J.-Y. Saillard, Coord. Chem. Rev. 178–180 (1998) 723–753.
[17] V. Babizhetskyy, K. Hiebl, Hj. Mattausch, A. Simon, J. Phys. Chem. Solid 70 (2009) 561-566.
[18] H. Hillebrecht, F.D. Meyer, Angew. Chem. Int. Ed. Engl. 35 (1996) 2499–2500.
[19] J.-F. Halet, J.-Y. Saillard, J. Bauer, J. Less-Common Met. 158 (1990) 239–250.
[20] Y. Shi, A. Leithe-Jasper, T. Tanaka, J. Solid State Chem. 184 (1999) 250–259.
[21] O. Oeckler, C. Jardin, Hj. Mattausch, A. Simon, J.-F. Halet, J.-Y. Saillard, J. Bauer, Z. Anorg. Allg. Chem. 627 (2001) 1389–1394.
[22] E. Bidaud, K. Hiebl, R.-D. Hoffman, R. Pöttgen, C. Jardin, J. Bauer, R. Gautier, P. Gougeon, J.-Y. Saillard, J.-F. Halet, J. Solid State Chem. 154 (2000) 286–295.
[23] T. Vomhof, R. Pöttgen, W. Jeitschko, J. Less-Common Met. 171 (1991) 95–99.
[24] E. Bidaud, K. Hiebl, J. Bauer, J. Alloys Compd. 279 (1998) 97–101.
[25] H.L. Krauss, H. Stack, Z. Anorg. Allg. Chem. 366 (1969) 34–42.
[26] N.W. Alcock, Crystallogr. Comput. (1970) 271.
[27] A. Altomare, M.C. Burla, M. Camalli, B. Carroccini, G.L. Cascarano, C. Giacovazzo, A. Guagliardi, A.G. Moliterni, G. Polidori, R. Rizzi, J. Appl. Crystallogr. 32 (1999) 115.
[28] G. M. Sheldrick, SHELXL-97, Program for the Refinement of Crystal Structures, University of Göttingen, Germany, 1997.
[29] L.J. Farrugia, WinGX (Version 1.64.05), J. Appl. Crystallogr. 32 (1999) 837–838.
[30] T. Roisnel, J. Rodríguez-Carvajal, WinPLOTR: a windows tool for powderdiffraction patterns analysis, in: R. Delhez, E.J. Mittenmeijer (Eds.), Proceedings of the 7th European Powder Diffraction Conference (EPDIC 7), Mater. Sci. Forum (2000) 118.
[31] J. Rodriguez-Carvajal, Phys. B. 192 (1993) 55.
[32] L.G. Akselrud, Yu.N. Grin, P.Yu. Zavalii, V.K. Pecharskii, WinCSD—universal program package for single crystal and/or powder structure data treatment, Mater. Sci. Forum 335 (1993) 133.
[33] S.D. Wijeyesekera, R. Hoffmann, Organometallics 3 (1984) 949–961.
[34] R. Hoffmann, J. Chem. Phys. 39 (1963) 1397–1412.
[35] M.H. Whangbo, R. Hoffmann, R.B. Woodward, Proc. R. Soc. London A 366 (1979) 23–46.
[36] V. Babizhetskyy, Hj. Mattausch, A. Simon, Z. Anorg. Allg. Chem. 635 (2009) 737–742.
[37] Hj. Mattausch, A. Simon, C. Felser, R. Dronskowski, Angew. Chem. Int. Ed. Engl. 35 (1996) 1685–1687.

[38] Hj. Mattausch, O. Oeckler, A. Simon, Inorg. Chim. Acta 289 (1999) 174–190.
[39] C. Jardin, O. Oeckler, Hj. Mattausch, A. Simon, J.-F Hallet, J.-Y. Saillard, J. Bauer, Inorg. Chem. 33 (2000) 5895–5900.
[40] C. Mealli, D.M. Proserpio, J. Chem. Educ. 67 (1990) 399–402.
[41] O. Oeckler, Doctoral Thesis, Universität Stuttgart, Germany, 2000.
[42] B. Barbara, V.N. Nguyen, E.S. Siaud, C. R. Seances Acad. Sci. Ser. C 274 (1972) 1053.